

**Inverse percolation by removing straight semirigid rods from bilayer square lattices**F. M. L. Pimentel <sup>1</sup>, N. De La Cruz Félix <sup>1,2</sup>, L. S. Ramirez <sup>2,3</sup> and A. J. Ramirez-Pastor <sup>2,\*</sup><sup>1</sup>*Instituto de Física (IFIS), Facultad de Ciencias, Universidad Autónoma de Santo Domingo–FONDOCYT, Av. Alma Mater, Santo Domingo 10105, Dominican Republic*<sup>2</sup>*Departamento de Física, Instituto de Física Aplicada (INFAP), Universidad Nacional de San Luis–CONICET, Ejército de Los Andes 950, D5700HHW, San Luis, Argentina*<sup>3</sup>*Instituto de Física Interdisciplinar y Sistemas Complejos (IFISC), Campus Universitat Illes Balears, Spain*

(Received 11 January 2023; accepted 7 June 2023; published 22 June 2023)

Numerical simulations and finite-size scaling analysis have been carried out to study the problem of inverse percolation by removing semirigid rods from a  $L \times L$  square lattice that contains two layers (and  $M = L \times L \times 2$  sites). The process starts with an initial configuration where all lattice sites are occupied by single monomers (each monomer occupies one lattice site) and, consequently, the opposite sides of the lattice are connected by nearest-neighbor occupied sites. Then the system is diluted by removing groups of  $k$  consecutive monomers according to a generalized random sequential adsorption mechanism. The study is conducted by following the behavior of two critical concentrations with size  $k$ : (1) jamming coverage  $\theta_{j,k}$ , which represents the concentration of occupied sites at which the jamming state is reached, and (2) inverse percolation threshold  $\theta_{c,k}$ , which corresponds to the maximum concentration of occupied sites for which connectivity disappears. The obtained results indicate that (1) the jamming coverage exhibits an increasing dependence on the size  $k$ —it rapidly increases for small values of  $k$  and asymptotically converges towards a definite value for infinitely large  $k$  sizes  $\theta_{j,k \rightarrow \infty} \approx 0.2701$ —and (2) the inverse percolation threshold is a decreasing function of  $k$  in the range  $1 \leq k \leq 17$ . For  $k \geq 18$ , all jammed configurations are percolating states (the lattice remains connected even when the highest allowed concentration of removed sites is reached) and, consequently, there is no nonpercolating phase. This finding contrasts with the results obtained in literature for a complementary problem, where straight rigid  $k$ -mers are randomly and irreversibly deposited on a square lattice forming two layers. In this case, percolating and nonpercolating phases extend to infinity in the space of the parameter  $k$  and the model presents percolation transition for the whole range of  $k$ . The results obtained in the present study were also compared with those reported for the case of inverse percolation by removal of rigid linear  $k$ -mers from a square monolayer. The differences observed between monolayer and bilayer problems were discussed in terms of vulnerability and network robustness. Finally, the accurate determination of the critical exponents  $\nu$ ,  $\beta$ , and  $\gamma$  reveals that the percolation phase transition involved in the system has the same universality class as the standard percolation problem.

DOI: [10.1103/PhysRevE.107.064128](https://doi.org/10.1103/PhysRevE.107.064128)**I. INTRODUCTION**

The percolation phase transition occurring in random sequential adsorption (RSA) models of extended objects is one of the most important subjects in statistical physics [1–5]. In this type of study, the objects are randomly and irreversibly deposited forming a single monolayer. The final state generated is a disordered state (known as jamming state), in which no more objects can be deposited due to the absence of free space of appropriate size and shape [4].

At intermediate densities, and under certain conditions, a transition occurs in the connectivity of the system [3]. The central idea of the percolation theory is based in finding the minimum concentration of occupied sites for which a cluster extends from one side to the opposite one of the system (a cluster is a group of occupied sites arranged in such a way that

each one of them has at least one occupied nearest-neighbor site). This particular value of the concentration rate is named critical concentration or percolation threshold and determines a well-defined second order transition in the system. Thus a competition between percolation and jamming is established.

The interplay between jamming and percolation is relevant for the description of deposition processes. Let us consider the deposition of objects of characteristic length  $k$ : straight rigid  $k$ -mers,  $k \times k$  square tiles, and  $k \times k \times k$  cubic blocks. Depending on the relationship between the dimension of the deposited object and the dimension of the substrate, the following different behaviors have been observed.

(i)  $D$ -dimensional lattice and  $D$ -dimensional depositing object. The percolation threshold is an increasing function of the size  $k$  in the range  $2 \leq k \leq k_{\max}$ . For  $k > k_{\max}$ , all jammed configurations are nonpercolating states and, consequently, the percolation phase transition disappears. Thus (1)  $k_{\max} = 1$  for straight rigid  $k$ -mers on 1D lattices [3,4], (2)  $k_{\max} = 3$  for  $k \times k$  square tiles ( $k^2$ -mers) on 2D square lattices [6–8], and

\*antorami@unsl.edu.ar

(3)  $k_{\max} = 16$  for  $k \times k \times k$  cubic objects ( $k^3$ -mers) deposited on 3D simple cubic lattices [9].

(ii)  $D$ -dimensional lattice and  $(D - 1)$ -dimensional depositing object. The percolation threshold is a nonmonotonic function of the size  $k$ ; it decreases for small particle sizes, goes through a minimum around  $k = k_{\min}$ , and finally tends to a constant value for large  $k$ 's. In other words, the percolation phase transition occurs for all values of  $k$ . Thus  $k_{\min} = 13$ , 11, and 48 for straight rigid  $k$ -mers on 2D square [10–12], triangular [13], and honeycomb [14] lattices, respectively, and  $k_{\min} = 18$  for  $k^2$ -mers on 3D simple cubic lattices [15].

(iii)  $D$ -dimensional lattice and  $(D - 2)$ -dimensional depositing object. This case corresponds to straight rigid  $k$ -mers on 3D simple cubic lattices. The percolation threshold shows a monotonic decrease with the size  $k$  and remains below the curve of jamming coverage versus  $k$ . Consequently, percolating and nonpercolating phases extend to infinity in the space of the parameter  $k$  and the model presents percolation transition in all ranges of said value [16].

Recently, the concept of inverse percolation has been introduced as a strategy to address connectivity loss in diluted lattices [17]. The study of the inverse percolation problem starts with all lattice sites occupied by single monomers (each monomer occupies one lattice site). Consequently, there always exists a spanning path through a sequence of nearest-neighbor occupied sites in the initial configuration. Then the system is diluted by randomly removing objects from the surface. The main objective is to obtain the maximum concentration of occupied sites (minimum concentration of empty sites) at which the connectivity disappears. This value of the concentration is named the inverse percolation threshold. The term inverse is used simply to indicate that the size of the conductive phase diminishes during the removal process and the percolation transition occurs between a percolating and a nonpercolating state.

The inverse percolation scheme can be used to describe the response of a network to the removal of sites or bonds, which is the phenomena of primary interest in robustness [18–23]. The model also offers a simplified representation of an irreversible reaction-annihilation process [24], where  $k$  nearest-neighbor particles react and desorb from the surface, leaving behind  $k$  empty sites ( $A^{(1)} + A^{(2)} + \dots + A^{(k)} \rightarrow 0$ ).

As in the classic percolation problem, the behavior of the inverse percolation threshold depends strongly on the structure, shape, and size of the removed objects and the geometry of the lattice. Several works have been developed in this line [13,17,25,26]. In the case of straight rigid  $k$ -mers removed from 2D square lattices [17], simulation results showed a nonmonotonic size  $k$  dependence for the inverse percolation threshold, which rapidly decreases for small particle sizes ( $1 \leq k \leq 3$ ). Then, it grows for  $k = 4, 5$ , and 6, goes through a maximum at  $k = 7$ , and finally decreases again and asymptotically converges towards a definite value for large values of  $k$ . The inverse critical concentration also exhibits a nonmonotonic behavior for the case of straight rigid  $k$ -mers removed from 2D triangular lattices [13,25]: it grows from  $k = 1$  to  $k = 10$ , presents a maximum at  $k = 11$ , and finally decreases and asymptotically converges towards a finite value for large segments. In both square and triangular lattices, the percolating and nonpercolating phases extend to infinity in the space

of the parameter  $k$  and, consequently, the model presents percolation transition in all the ranges of  $k$ -mer size.

The situation is very different for the problem of inverse site percolation by the removal of  $k \times k$  square tiles ( $k^2$ -mers) from 2D square lattices [26]: the inverse percolation threshold is a decreasing function of  $k$  in the range ( $1 \leq k \leq 4$ ). For  $k \geq 5$ , all jammed configurations are percolating states and, consequently, the percolation transition disappears (the lattice remains connected even when the highest allowed concentration of removed sites is reached).

The aforementioned studies have been conducted in the monolayer regime; however, less attention has been received by the development of more realistic models considering the formation of more than one layer. In a recent work from our group [27], the irreversible bilayer adsorption of straight semirigid  $k$ -mers of different sizes on 2D square lattices has been studied. The adsorption kinetics was simulated by a RSA algorithm, generalized to two deposited layers. The obtained results revealed that the percolation threshold exhibits a monotonic decreasing function when it is plotted as a function of the  $k$ -mer size. This behavior is completely different from that observed for the monolayer problem, where the percolation threshold shows a nonmonotonic  $k$ -mer size dependence.

The study in Ref. [27] clearly shows that the bilayer formation drastically affects the behavior of the percolation threshold with  $k$  and other critical properties (such as the crossing points of the percolation probability functions). The notable differences observed between monolayer and bilayer problems for standard percolation encourage the extension of the inverse percolation model to substrates formed by more than one layer. The objective of this paper is to provide a thorough study in this direction. For this purpose, extensive numerical simulations supplemented by analysis using finite-size scaling theory have been carried out to study the problem of inverse percolation by removing semirigid rods from square bilayers. Jamming and percolation thresholds have been obtained as a function of the  $k$ -mer size. In addition, an exhaustive analysis of critical exponents and universality has been performed. All of these quantities are reported for the bilayer problem.

The percolation problem in the bilayer may resemble the case of percolation on multilayer networks [28–33]. These systems consist of two interdependent networks, denoted as  $A$  and  $B$ , with a common number  $M$  of nodes. The functioning of a node in network  $A$ , denoted as  $A_i$  [where  $i = (1, \dots, M)$ ], is dependent on the performance of the corresponding node in network  $B$ , denoted as  $B_i$ . Specifically, a failure in a node  $A_i$  leads to a cessation of the operation of the corresponding node  $B_i$ , highlighting the interdependence of the networks. Given that many critical infrastructures such as power stations, transportation, and power grids are interconnected, the study of multiplex networks has become increasingly important displaying differences in terms of their robustness and percolation characteristics when compared to single networks [34]. Although some similarities can be found between the interdependent networks and bilayer problems, there are substantial differences in the dilution process. In interdependent networks, the failures of nodes in one network cause dependent nodes in the other network to fail, leading to a cascade of failures [34]. However, in our inverse percolation problem,

the removal of a particle  $(i, j, 1)$  in the upper layer is required to remove the particle beneath it,  $(i, j, 2)$ , but these are not simultaneous events. Furthermore, the particle in  $(i, j, 2)$  may never be removed due to jamming.

Another variation of the classical percolation problem in which components of the system are also removed randomly, irreversibly, and independently until large scale connectivity is lost was given in Ref. [35], where the authors introduced the “drilling percolation” model. The problem consists of studying how a solid cube is randomly drilled until it fragments into pieces. For this purpose, columns of size  $1 \times 1 \times L$  are sequentially removed from a large cube of size  $L \times L \times L$ . The process is repeated until the structure collapses into small pieces and the bottom and top part of the cube are no longer connected. The drilling percolation model exhibits a continuous transition at a critical density of holes with a different universality than the random percolation [35–37]. It should be noted that the problem presented here is different from the one in Ref. [35], not only in terms of the structure (bilayer  $2 \times L \times L$ /cube  $L \times L \times L$ ), but also in terms of the removal process (needles of size  $k \ll L$ /rods of size  $L$ ).

This paper is organized as follows. The deposition model and jamming results are described in Sec. II. The percolation properties (inverse percolation thresholds and critical exponents) are presented and discussed in Sec. III. Finally, the conclusions are drawn in Sec. IV.

**II. MODEL, REMOVAL KINETICS, AND JAMMING COVERAGE**

Let us assume the substrate is represented by a two-dimensional  $L \times L$  square lattice that contains two layers, so that the sites matrix has a geometry  $M = L \times L \times 2$ . Occupied and empty sites are distributed with concentrations  $\theta$  and  $\theta^*$  ( $\theta^* = 1 - \theta$ ), respectively. Initially, all sites are occupied; thus the concentration is  $\theta = 1$  ( $\theta^* = 0$ ). When  $N$   $k$ -mers are removed, the concentration of occupied [empty] sites goes as  $\theta = 1 - kN/(2L^2)$  [ $\theta^* = kN/(2L^2)$ ].

The surface goes through a dilution process in which groups of  $k$  particles are removed at a time. Those groups of particles are sets of consecutive occupied sites aligned along one of two lattice axes and are called  $k$ -mers. The positions available for desorption are indicated by three indices  $(i, j, n)$ . The pair  $(i, j)$  denotes the location in the square lattice ( $x, y$  coordinates) and  $n$  is the layer number:  $n = 1$  for layer 1 (bottom layer) and  $n = 2$  for layer 2 (top layer).

The desorption process starts by the removal of a  $k$ -mer from the top layer. After this first  $k$ -mer is removed, the system is randomly diluted as follows: (i) one of the two  $(x, y)$  possible lattice directions and a starting site are randomly chosen and (ii) if, beginning at the chosen site, there are  $k$  consecutive nearest-neighbor sites (particles), then a  $k$ -mer is removed from those sites (see Fig. 1). Otherwise, the attempt is rejected. The removal procedure is performed with periodic boundary conditions in both directions ( $x$  and  $y$  axes) and in both layers. For a given realization, we start from a fully occupied lattice with  $\theta = 1$  and remove  $k$ -mers until no more removals are possible. Every time  $\bar{N}$   $k$ -mers are removed [that is, the concentration of occupied sites decreases in a  $\Delta\theta = k\bar{N}/(2L^2)$ ], the percolation and jamming quantities that

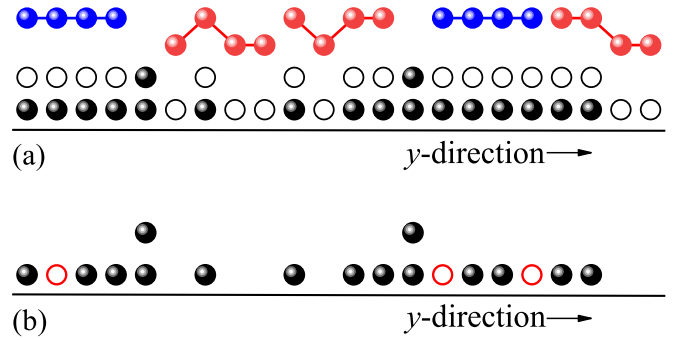


FIG. 1. (a) Schematic representation of tetramers ( $k = 4$ ) removed along a line in the  $y$  direction of the square lattice. As the  $k$ -mers are semirigid, they can deform to find adjacent empty sites between the second and first layers (but always extend along one of the two lattice directions). Black spheres not connected represent initially filled sites, open black spheres not connected represent vacancies, blue spheres connected by lines correspond to  $k$ -mers in the second layer, and red spheres connected by lines indicate  $k$ -mers located partially in the first and second layers. (b) Final state. Some objects have been removed in the  $x$  direction (open red circles). The system has reached the jamming state and it is no longer possible to remove objects of length 4.

are described below are measured. This strategy allows us to get information for several values of  $\theta$  in a single run. To obtain statistically meaningful results, we repeat this process  $10^5$  times and calculate the average percolation and jamming quantities. This averaging over many realizations allows us to obtain reliable results.

A simple visualization of how the lattice is diluted is presented in Fig. 1(a). The figure shows a portion of sites along the  $y$  direction of a square lattice.  $k$ -mers (with  $k = 4$ ) removed from the top layer are indicated by blue spheres connected by lines. The dilution is not restricted to straight rigid rods but includes semirigid  $k$ -mers whose components may be in both layers. The removed semirigid objects are denoted as red spheres connected by lines. The resulting vacancies are indicated by open black spheres not connected. Black spheres not connected represent occupied sites. As shown in the figure, removing a  $k$ -mer unit from a given  $(i, j, 1)$  site in the bottom layer requires that the site  $(i, j, 2)$  in the top layer has already been removed. In part (b), the final state is presented. Open red circles represent vacancies generated by  $k$ -mers removed along the  $x$  direction. In the final state, it is no longer possible to remove objects of length 4.

The removal process ends when there are no  $k$ -adjacent occupied sites to remove; see Fig. 1(b). The coverage at which it is no longer possible to remove units even when there are occupied sites is called jamming coverage. This configuration depends both on the size of the deposited object and the lattice geometry. In order to find the maximum concentration  $\theta$  for which the connectivity disappears, the space of concentrations allowed for removal given by the jamming concentration must be known.

As it was established in Refs. [17,25], both the direct and inverse jamming problems are complementary for the monolayer and it is possible to obtain one from the other. This argument can be extended for the bilayer as follows. Let us

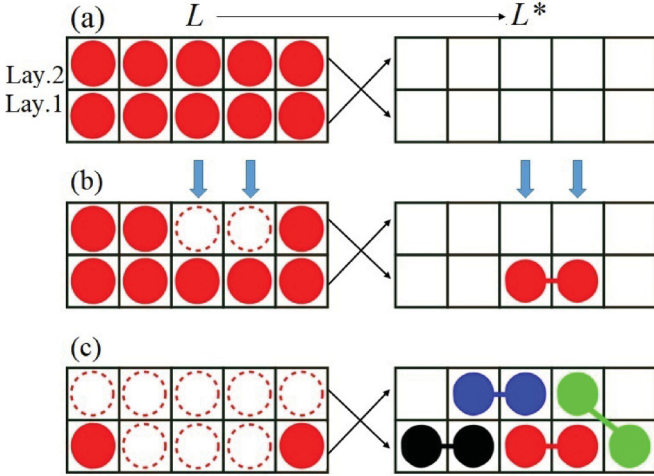


FIG. 2. Mapping  $L \rightarrow L^*$  from the original bilayer lattice  $L$  to the complementary lattice  $L^*$  where the first (second) layer in  $L$  corresponds to the second (first) layer in  $L^*$  and each empty (occupied) site of  $L$  transforms into an occupied (empty) one of  $L^*$ . Three different situations have been represented: (a)  $L$  is fully occupied thus  $L^*$  is empty, (b) a dimer has been removed from the second layer of  $L$  and then it corresponds to the deposition of a dimer in the first layer of  $L^*$ , and (c) a set of dimers are removed from  $L$  so that no more objects can be removed and, consequently, no more objects fit in  $L^*$ . Full circles correspond to the occupied sites and the dotted circles to the removed objects.

consider a mapping  $L \rightarrow L^*$  from the original bilayer lattice  $L$  to the complementary lattice  $L^*$  where the first (second) layer in  $L$  corresponds to the second (first) layer in  $L^*$  and each empty (occupied) site of  $L$  transforms into an occupied (empty) one of  $L^*$ ; see Fig. 2(a). The latter can be better appreciated in Fig. 2(b), which shows how the removal of a dimer in the second layer of  $L$  maps to a dimer deposition in the first layer of  $L^*$ . Then, the filling process in the complementary lattice (dilution process in the original lattice) is equivalent to a RSA process of  $k$ -mers. Accordingly, the final state in  $L^*$  is a disordered state (known as jamming state), in which no more objects can be deposited due to the absence of free space of appropriate size and shape [4] [see Fig. 2(c)].

The jamming threshold as a function of  $k$  ( $\theta_{j,k}^*$ ) was obtained in Ref. [27] for the deposition of semirigid  $k$ -mers on a bilayer square lattice. The authors found that (1)  $\theta_{j,k}^*$  is a decreasing function of  $k$  and (2) the best fit to  $\theta_{j,k}^*$  (obtained for  $k \geq 8$ ) corresponds to the expression  $\theta_{j,k}^* = 0.7299 - 0.062/k + 3.54/k^2$ , with  $\theta_{j,\infty}^* = 0.7299(21)$  being the result for the limit coverage of a square bilayer lattice by infinitely long  $k$ -mers.

Then, during the dilution process in the original lattice, the fraction of holes varies between 0 and  $\theta_{j,k}^*$ , while the fraction of occupied sites ranges from 1 to  $\theta_{j,k}$  ( $\equiv 1 - \theta_{j,k}^*$ ) as

$$\theta_{j,k} = 0.2701 + \frac{0.062}{k} - \frac{3.54}{k^2} \quad (k \geq 8). \quad (1)$$

Once the space of the parameters  $\theta$  and  $\theta^*$  are determined, the percolation properties of the system will be studied in the following.

### III. PERCOLATION PROPERTIES

As already mentioned, the central idea of inverse percolation is based on finding the maximum concentration of occupied sites,  $\theta$ , for which connectivity disappears. This critical concentration is called inverse percolation threshold  $\theta_c$  and determines a well defined geometrical transition that separates a phase in which an infinite cluster is present ( $\theta > \theta_c$ ) from a phase where we find many finite clusters ( $\theta < \theta_c$ ). This is a second-order phase transition and can be characterized by well-defined critical exponents. Our interest is in studying the bilayer problem and in determining (i) how the inverse percolation threshold is modified when the size of the  $k$ -mer increases and (ii) to what universality class the phase transition of this problem belongs.

#### A. Calculation method

It is well known that it is quite a difficult matter to analytically determine the value of a percolation threshold for a given lattice when multisite occupation is considered. Then, percolation thresholds have to be estimated numerically by means of computer simulations.

To obtain the inverse percolation threshold, we perform a number of numerical simulations of the following steps: (a) the construction of the bilayer lattice for the desired fraction  $\theta$  of occupied sites, according to the scheme in Sec. II, and (b) the cluster analysis by using the Hoshen and Kopelman algorithm [38] with the following connectivity criterion: each position  $(i, j, 1)$  in the first layer has four nearest-neighbor positions in the first layer  $[(i - 1, j, 1), (i + 1, j, 1), (i, j - 1, 1), \text{ and } (i, j + 1, 1)]$  and one nearest-neighbor position in the second layer  $[(i, j, 2)]$ . In the same way, each position  $(i, j, 2)$  in the second layer has four nearest-neighbor positions in the second layer  $[(i - 1, j, 2), (i + 1, j, 2), (i, j - 1, 2), \text{ and } (i, j + 1, 2)]$  and one nearest-neighbor position in the first layer  $[(i, j, 1)]$  and (c) the determination of the largest cluster  $S_L$  and, finally, the existence of a percolating island. In steps (b) and (c), open boundary conditions are implemented. At this point, the probability  $R_{L,k}^X(\theta)$  that a bilayer lattice composed of  $L \times L \times 2$  sites percolates at the concentration  $\theta$  of occupied sites is calculated. According to the aforementioned connectivity criterion, we say that a bilayer lattice percolates when there is a percolating path (composed by nearest-neighbor occupied sites located in layer 1 and layer 2) that passes from one side to the other side of the system. The subindex  $k$  in the definition of  $R$  indicates that the density  $\theta$  was reached by removing sets of particles of size  $k$  ( $k$ -mers).

The probability  $R = R_{L,k}^X(\theta)$  that a bilayer lattice of linear size  $L$  percolates at concentrations  $\theta$  is defined [39] as follows.

$R_{L,k}^R(\theta)$ : the probability of finding a rightward percolating cluster, along the  $x$  direction.

$R_{L,k}^D(\theta)$ : the probability of finding a downward percolating cluster, along the  $y$  direction.

$R_{L,k}^U(\theta)$ : the probability of finding a cluster which percolates on any direction.

$R_{L,k}^I(\theta)$ : the probability of finding a cluster which percolates in both (mutually perpendicular) directions.

$$R_{L,k}^A(\theta) = \frac{1}{2}[R_{L,k}^U(\theta) + R_{L,k}^I(\theta)].$$

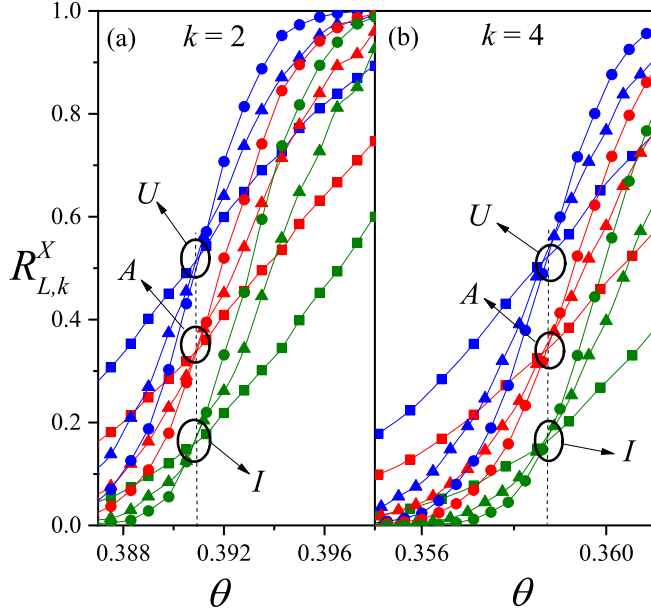


FIG. 3. Fraction of percolating lattices  $R_{L,k}^X(\theta)$  as a function of the concentration  $\theta$  for  $k = 2$  (a),  $k = 4$  (b), and three different lattice sizes:  $L/k = 128$ , squares,  $L/k = 320$ , triangles, and  $L/k = 512$ , circles. Blue, red, and green symbols represent data for  $U$ ,  $A$ , and  $I$  criteria, respectively. Vertical dashed lines denote the inverse percolation threshold in the thermodynamic limit  $L \rightarrow \infty$ .

A total of  $m_L = 10^5$  independent runs of such a two step procedure were carried out for each bilayer of size  $L$ . Then,  $R_{L,k}^X(\theta)$  is given by the number of samples that have a percolating cluster for a given criterion  $X = \{R, D, I, U, A\}$ ,  $m_L^X$ , divided by the total number of samples:  $R_{L,k}^X(\theta) = m_L^X/m_L$ . The procedure is repeated for different values of  $L$ ,  $\theta$ , and  $k$ -mer size. In our simulations,  $2 \leq k \leq 20$  and  $0 \leq \theta \leq \theta_j$ . In the case of  $k \leq 12$ , the values of the inverse percolation thresholds were obtained for lattice sizes  $L/k = 128, 256, 320, 448, \text{ and } 512$ . The cases corresponding to  $k$  ranging between 14 and 20 were calculated for  $L/k = 64, 96, 128, \text{ and } 256$  with an effort reaching almost the limits of our computational capabilities. As it can be appreciated, this represents extensive calculations from the numeric point of view.

In addition to the different probabilities  $R_{L,k}^X(\theta)$ , percolation order parameter  $P$  and susceptibility  $\chi$  have been measured [40–42] as

$$P = \frac{\langle S_L \rangle}{M} \quad (2)$$

and

$$\chi = [\langle S_L^2 \rangle - \langle S_L \rangle^2]/M, \quad (3)$$

where  $M = 2L^2$ ,  $S_L$  represents the size of the largest cluster, and  $\langle \dots \rangle$  means an average over simulation runs.

## B. Percolation thresholds

In Fig. 3, the probabilities  $R_{L,k}^A(\theta)$ ,  $R_{L,k}^I(\theta)$ , and  $R_{L,k}^U(\theta)$  are presented for  $k = 2$  (a) and  $k = 4$  (b). As mentioned above, the simulations were performed for lattice sizes ranging

between  $L/k = 128$  and  $L/k = 512$ . For clarity, simulation results from only three lattice sizes are shown:  $L/k = 128$  (squares),  $L/k = 320$  (up triangles), and  $L/k = 512$  (circles). The behavior of the probability curves  $R_{L,k}^X(\theta)$  strongly depends on the system size. Even so, for a given criterion  $X$ , they all cross in a unique point  $R^{X*}$ . In this case, the obtained values  $R^{A*} \approx 0.35$ ,  $R^{I*} \approx 0.17$ , and  $R^{U*} \approx 0.53$  agree with the ones reported for the standard percolation bilayer problem [27]. In addition, the intersection points do not modify their numerical value for the different  $k$  sizes studied. This finding represents an indication that the universality class of the phase transition involved in the inverse percolation bilayer problem (i) does not change with respect to the standard percolation bilayer problem and (ii) is conserved no matter the values of  $k$ .

The crossing point for each criterion  $X$  is located at a very well defined value in the  $\theta$  axis, allowing for a preliminary calculation of the inverse percolation threshold. The theory of finite-size scaling [3,40] gives us a more efficient way to determine the percolation threshold from the maximum of the curves of  $R_{L,k}^X(\theta)$ . To do this, first it is convenient to fit the probability curves with some function through the least-squares method so that they can be expressed as a continuous function of  $\theta$ . The fitting curve used is the *error function* because  $dR_{L,k}^X(\theta)/d\theta$  is expected to behave like the Gaussian distribution near the peak. This assumption is good enough to obtain the parameters that are needed to apply finite-size scaling theory [3,43],

$$\frac{dR_{L,k}^X(\theta)}{d\theta} = \frac{1}{\sqrt{2\pi} \Delta_{L,k}^X} \exp \left\{ -\frac{1}{2} \left[ \frac{\theta - \theta_{c,k}^X(L)}{\Delta_{L,k}^X} \right]^2 \right\}, \quad (4)$$

where  $\theta_{c,k}^X(L)$  is the concentration at which the slope of  $R_{L,k}^X(\theta)$  is the largest and  $\Delta_{L,k}^X$  is the standard deviation from  $\theta_{c,k}^X(L)$ . For large systems ( $L \rightarrow \infty$ ), these thresholds converge to a unique value according to the scaling behavior [3]

$$\theta_{c,k}^X(L) = \theta_{c,k}^X(\infty) + A^X L^{-1/\nu}, \quad (5)$$

where  $A^X$  is a nonuniversal constant and  $\nu$  is the critical exponent of the correlation length.

Figure 4 shows the plots towards the thermodynamic limit of the inverse percolation threshold  $\theta_{c,k}^X(L)$  according to Eq. (5) for the data in Fig. 3. The critical exponent  $\nu$  was set as  $\nu = 4/3$  for the present analysis, since, as will be shown in Sec. III C, our model belongs to the same universality class as random percolation [3]. From extrapolations it is possible to obtain  $\theta_{c,k}^X(\infty)$  for the criteria  $I$ ,  $A$ , and  $U$ . Combining the three estimates for each case, the final values of  $\theta_{c,k}(\infty)$  can be obtained. The maximum of the differences between  $|\theta_{c,k}^U(\infty) - \theta_{c,k}^A(\infty)|$  and  $|\theta_{c,k}^I(\infty) - \theta_{c,k}^A(\infty)|$  gives the error bar for each determination of  $\theta_{c,k}(\infty)$ . In this case, the values obtained were  $\theta_{c,k=2}(\infty) = 0.3910(3)$  and  $\theta_{c,k=4}(\infty) = 0.3587(2)$ . For the rest of the paper, we will denote the percolation threshold for each size  $k$  by  $\theta_{c,k}$  [for simplicity we will drop the symbol “( $\infty$ )”].

The method used in Fig. 4 was introduced by Yonezawa *et al.* [39] to estimate percolation thresholds from the study of finite-size systems. In Ref. [39], the authors showed that (1) a true value close to the percolation threshold of an infinite

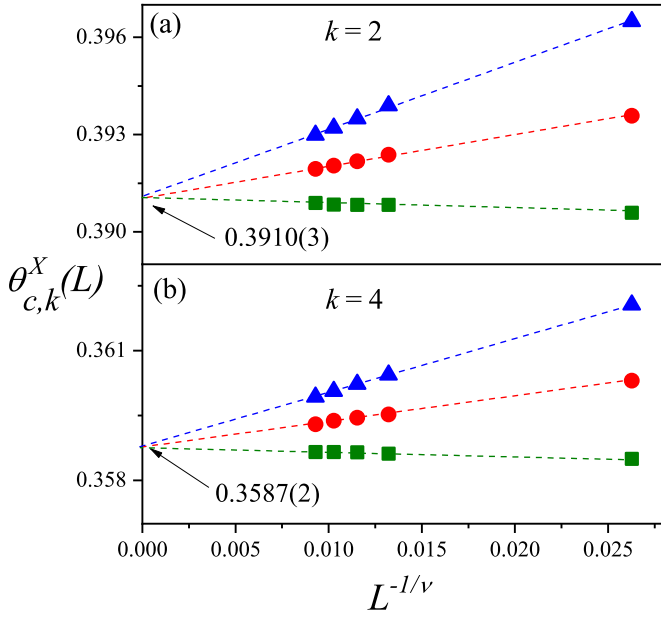


FIG. 4. Extrapolation of the inverse percolation threshold for an  $L$ -lattice  $\theta_{c,k}^X(L)$  ( $X = I, A, U$ ) toward the thermodynamic limit according to the theoretical prediction given by Eq. (5). Squares, circles, and triangles denote the values of  $\theta_{c,k}^X(L)$  obtained by using the criteria  $I, A$ , and  $U$ , respectively. Two values of  $k$  are presented: (a)  $k = 2$  and (b)  $k = 4$ . The bar error in each measurement is smaller than the size of the corresponding symbol.

system can be obtained from the probability curves for  $A$  criterion and (2) upper and lower bounds of the estimated threshold are given from the probability curves for  $I$  and  $U$  criteria, respectively.

The procedure of Fig. 4 was repeated for increasing values of  $k$ . The obtained results revealed that the inverse percolation threshold is a monotonically decreasing function of  $k$  in the interval  $[1, 17]$  (see Fig. 7). However, when  $k$  increases above 17 ( $k > 17$ ), a striking behavior is observed: all jammed configurations are percolating states and, consequently, there is no nonpercolating phase. This phenomenon can be better understood by examining Fig. 5, where the curves of  $R_{L,k}^X(\theta)$  ( $X = I, U, A$  as indicated) as a function of the concentration  $\theta$  are shown for  $k = 17$  (a) and  $k = 18$  (b).

For  $k = 17$ , three lattice sizes are shown in the figure:  $L/k = 96$  (squares),  $L/k = 128$  (triangles), and  $L/k = 256$  (circles). The probabilities  $R_{L,k}^A(\theta)$ ,  $R_{L,k}^I(\theta)$ , and  $R_{L,k}^U(\theta)$  look similar to those of Fig. 3. Namely, the curves for different lattice sizes cross each other in a unique point (which depends on the criterion  $X$  used), determining the inverse percolation threshold for each  $k$ .

The situation is different for  $k = 18$ . In this case, only the curves for  $L/k = 128$  (triangles) and  $L/k = 256$  (circles) are plotted. As it can be observed from Fig. 5(b) (and from data not shown here for clarity), the functions  $R_{L,k}^X(\theta)$  tend to 1 as the lattice size increases. Thus it is expected that, in the thermodynamic limit ( $L \rightarrow \infty$ ), the probabilities  $R_{L,k}^X(\theta)$  remain constant and equal to 1 up to the jamming coverage  $\theta_{j,k=18} = 0.2632(1)$  (vertical dashed line in the figure). This finding is a clear indication that (i) the percolation phase

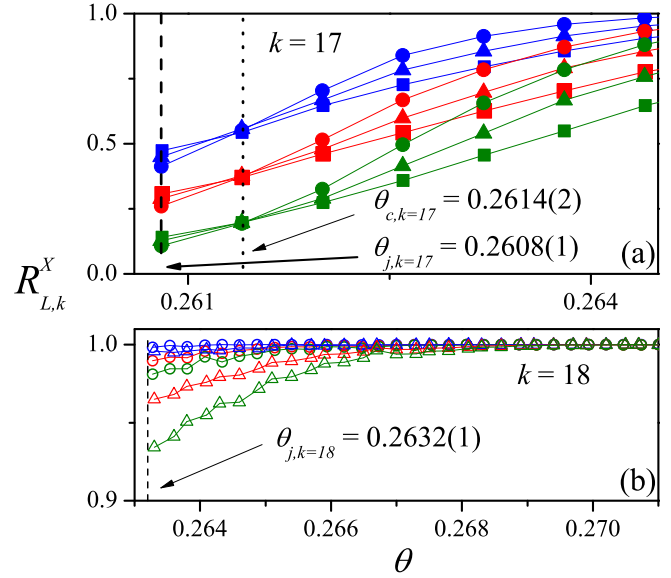


FIG. 5. (a) Fraction of percolating lattices  $R_{L,k}^X(\theta)$  as a function of the concentration  $\theta$  for  $k = 17$  and different lattice sizes:  $L/k = 96$  (squares),  $128$  (triangles), and  $256$  (circles). Blue, red, and green symbols represent data for  $U, A$ , and  $I$  criteria, respectively. Dashed and dotted lines denote the inverse jamming limit and the percolation threshold in the thermodynamic limit  $L \rightarrow \infty$ , respectively. (b) Same as part (a) but for  $k = 18$ . For clarity, only the curves for  $L/k = 128$  (triangles) and  $L/k = 256$  (circles) are plotted. The vertical dashed line indicates the inverse jamming coverage.

transition disappears and (ii) there is only one phase (the percolating phase) for  $k > 17$ . The interplay between the percolation and the jamming effects is responsible for the existence of a maximum value of  $k$  (in this case,  $k_{\max} = 17$ ) from which the percolation phase transition no longer occurs. These concepts can be better visualized with the help of the next figure.

Figure 6 shows typical configurations obtained after removing semirigid  $k$ -mers from a  $32 \times 32 \times 2$  square bilayer lattice. Gray (black) spheres represent occupied sites in the first (second) layer. Green and yellow lines indicate percolation paths connecting top and bottom (left and right) sides of the lattice. In part (a),  $k = 16 < k_{\max}$ , the fraction of occupied sites is slightly above the corresponding jamming coverage and the system percolates in both directions. Solid spheres surrounded by ellipses correspond to sets of 16 consecutive nearest-neighbor sites, which could still be removed from the lattice. Now suppose that the dilution process continues and the set of sites pointed to by an arrow is removed. The obtained configuration [see Fig. 6(b)] corresponds to a nonpercolating state (note that vertical and horizontal connectivity disappeared) and the jamming concentration has not yet been reached. A percolation phase transition has occurred during the removal process.

The same does not happen for the case of  $k > k_{\max}$ . In fact, Fig. 6(c) depicts a typical jamming configuration produced by the removal of  $k$ -mers of length  $k = 20 > k_{\max}$ . Upon reaching jamming, there is no possibility of removing 20-mers, but the lattice is still connected by occupied sites. In this case,

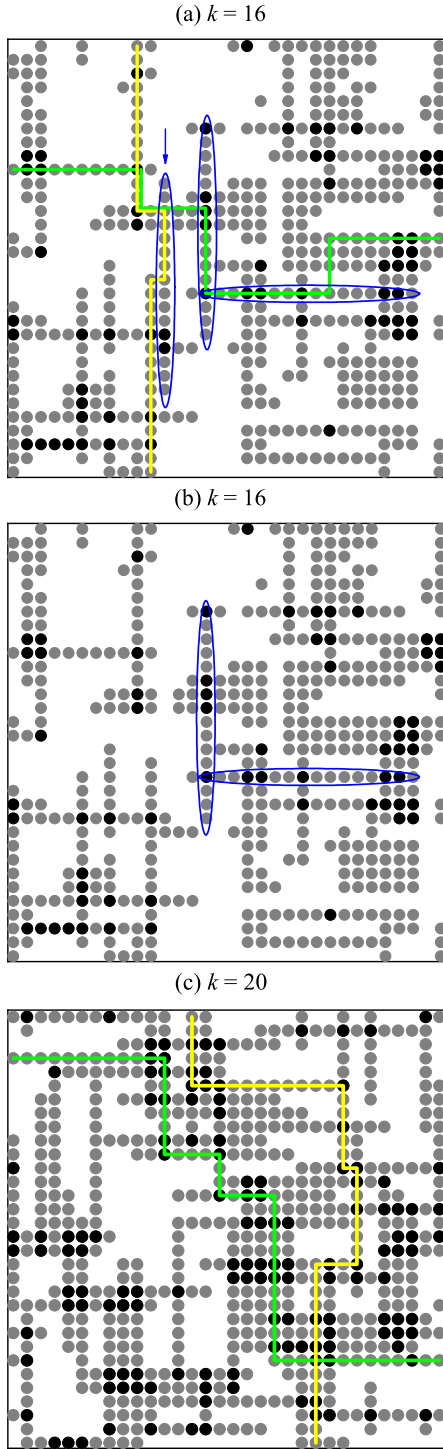


FIG. 6. Typical configurations obtained after removing semirigid  $k$ -mers from a  $32 \times 32 \times 2$  square lattice at the bilayer regime. Gray (black) spheres represent occupied sites in the first (second) layer. Green and yellow lines indicate percolation paths connecting top and bottom (left and right) sides of the lattice. In part (a),  $k = 16 < k_{\max}$  and the fraction of occupied sites is slightly above the corresponding jamming coverage. Solid spheres surrounded by ellipses correspond to sets of 16 consecutive nearest-neighbor sites, which could still be removed from the lattice. (b) Configuration obtained after removing the set of sites pointed to by an arrow in part (a). In part (c), a typical jamming configuration produced by the removal of  $k$ -mers of length  $k = 20 > k_{\max}$  is shown.

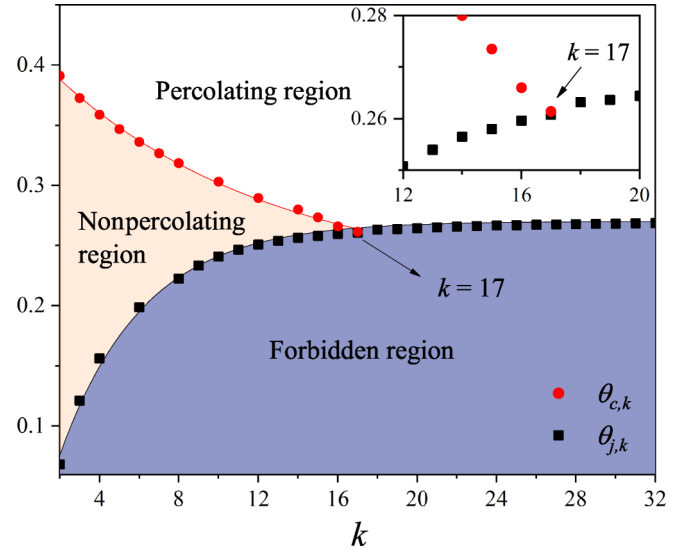


FIG. 7. Inverse percolation threshold  $\theta_{c,k}$  (solid circles) and jamming coverage  $\theta_{j,k}$  (solid squares) for  $k$  ranging from 2 to 32. The line fitting the solid squares corresponds to Eq. (1). Inset: zoom of the main figure for  $12 \leq k \leq 20$ .

the lattice connectivity is maintained throughout the entire removal process and no percolation phase transition occurs.

The resulting jamming-percolation phase diagram is presented in Fig. 7: (1) for  $1 \leq k \leq 17$ , the curve of  $\theta_{c,k}$  (solid circles) divides the space of allowed values of  $\theta$  in a percolating region ( $\theta > \theta_{c,k}$ ) and a nonpercolating region ( $\theta_{j,k} < \theta < \theta_{c,k}$ ) and (2) for  $k > 17$ , the entire space of allowed values of  $\theta$  ( $\theta > \theta_{j,k}$ ) is a percolating region. The region below the curve of  $\theta_{j,k}$  (solid squares) corresponds to a forbidden region for removal of the  $\theta$  space. The line fitting the solid squares corresponds to Eq. (1).

The decreasing behavior of  $\theta_{c,k}$  versus  $k$  is also accompanied by a decrease in the partial concentrations  $\theta_{c,k}^{11}$  and  $\theta_{c,k}^{12}$ , where  $\theta_{c,k}^{11}$  ( $\theta_{c,k}^{12}$ ) represents the coverage of the layer 1(2) at the critical point ( $\theta_{c,k} = \theta_{c,k}^{11}/2 + \theta_{c,k}^{12}/2$ ). The partial critical concentrations vary from  $\theta_{c,k=2}^{11} \approx 0.569$  and  $\theta_{c,k=2}^{12} \approx 0.213$  to  $\theta_{c,k=17}^{11} \approx 0.469$  and  $\theta_{c,k=17}^{12} \approx 0.053$ . These findings indicate that, in the percolating phase, most of the occupied sites are located in layer 1 (73% for  $k = 2$  and 90% for  $k = 17$ ) and only a minority of the occupied sites are in the layer 2. Then, if the layers are analyzed independently, (i) we observe always a percolating cluster in layer 1 when  $\theta = \theta_{c,k}$  (for all values of  $k$ ) and (ii) on the contrary, the layer 2 is a nonpercolating phase at the critical coverage  $\theta = \theta_{c,k}$  (occupied sites located in layer 2 can only be connected to each other through sites in layer 1).

In the case of the standard percolation bilayer problem [27], the percolation threshold is a decreasing function with increasing  $k$  [solid squares in Fig. 8(a)]. That is, the percolation threshold decreases for small particle sizes and then tends to a constant value for very long objects. Accordingly, the model presents percolation transition in all ranges of  $k$ -mer size. This monotonic decreasing behavior is completely different from that observed in Fig. 7 for the inverse percolation bilayer problem, where the percolation threshold curve cuts

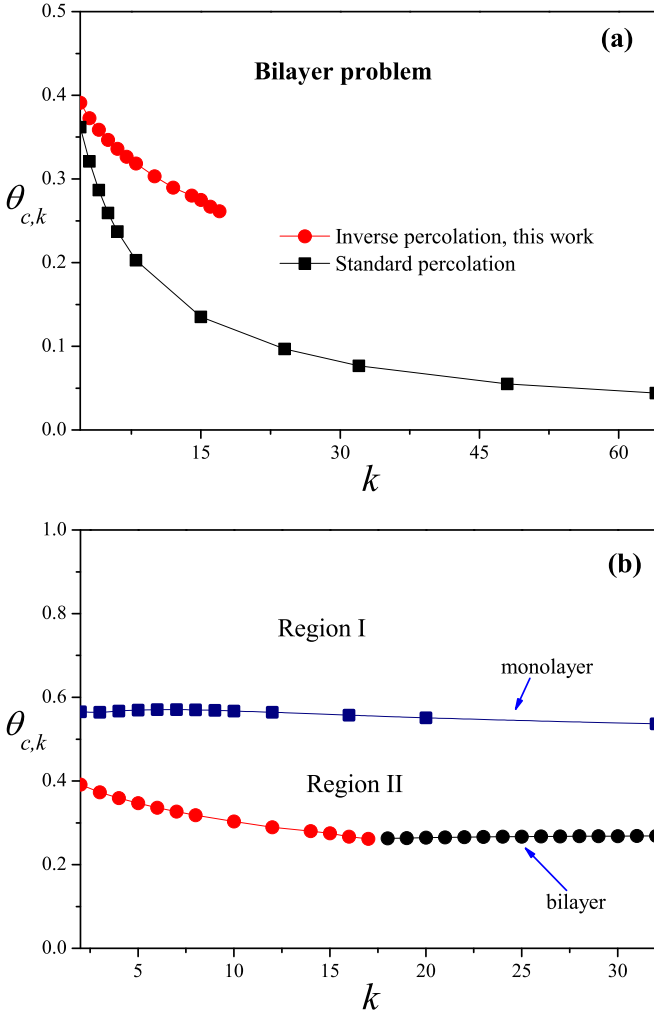


FIG. 8. (a) Inverse percolation curve in Fig. 7,  $\theta_{c,k}$  versus  $k$  (solid circles), is shown in comparison with the data of the standard percolation threshold as a function of size  $k$  corresponding to irreversible bilayer adsorption of straight semirigid  $k$ -mers on 2D square lattices (solid squares, Ref. [27]). (b) Comparison between the percolation phase diagram obtained by removing semirigid  $k$ -mers from square bilayers (solid circles) and the corresponding one obtained by removing rigid  $k$ -mers from square monolayers (solid squares) [17]. Region I represents the percolating region for the monolayer problem. In the case of the bilayer problem, the percolating region is the sum of regions I and II.

off abruptly at  $k = 17$  [solid circles in Fig. 8(a)]. Thus, while the inverse and direct jamming bilayer problems turn out to be complementary and, therefore, one can be deduced from the other ( $\theta_{j,k} + \theta_{j,k}^* = 1$ ; see Sec. II), the same is not true for the inverse and direct percolation bilayer problems.

Finally, it is also interesting to compare the results obtained here for the bilayer problem with those reported for the case of inverse percolation by removing rigid linear  $k$ -mers from a square monolayer [17]. The comparative study is shown in Fig. 8(b). Solid squares represent the inverse percolation threshold as a function of  $k$  for the square lattice. This curve was previously obtained in Ref. [17] and determines the lower limit of the percolating region for the monolayer problem. In the case of the bilayer problem, the lower boundary of the

percolating region (solid circles) results from the combination of two curves (see the phase diagram in Fig. 7): (i) the percolation curve for  $k$  ranging between 1 and 17 and (ii) the jamming curve for  $k > 17$ .

As it can be observed from Fig. 8(b), the limit curve corresponding to the bilayer problem remains below the curve obtained for the monolayer problem. This behavior has very interesting implications in terms of vulnerability and network attacks. In fact, inverse percolation theory can be used to understand network robustness, i.e., how the connectivity of a network changes as its elements (sites or bonds) are removed (or failed) through either random or malicious attacks [18–23]. The focus of robustness in complex networks is the response of the network to the removal of nodes or links. From this point of view, the results in Fig. 8(b) indicate that the square monolayer is more vulnerable than the square bilayer to removal of linear sets of consecutive nodes. As an illustrative example, it is necessary to remove almost 68% of the links to disconnect a bilayer lattice by removing sets of eight linear nearest-neighbor consecutive sites. The same effect can be achieved by removing only 43% of nodes in the case of a monolayer lattice. Moreover, for large  $k$ -mers ( $k > 17$ ), the bilayer lattice remains connected even when the highest allowed concentration of removed sites is reached.

### C. Critical exponents and universality

In order to determine the universality class to which this problem belongs, the critical exponents  $\nu$ ,  $\beta$ , and  $\gamma$  have been calculated. According to scaling assumptions, the standard finite size scaling theory [40] provides several ways to estimate the critical exponent  $\nu$  from simulation data. One of these methods is from the maximum of the function  $dR_{L,k}^X/d\theta$ ,

$$\left(\frac{dR_{L,k}^X}{d\theta}\right) \propto L^{1/\nu}. \quad (6)$$

In Fig. 9(a),  $\log[(dR_{L,k}^X/d\theta)_{\max}]$  has been plotted as a function of  $\log L$  (note the log-log functional dependence) for  $k = 2$  and 4 as indicated. According to Eq. (6), the slope of each line corresponds to  $1/\nu$ . As it can be observed, the slopes of the curves remain constant, with  $\nu = 4/3$  being for the inverse percolation model in the bilayer square lattice.

Once  $\nu$  was known, the exponent  $\gamma$  can be determined by scaling the maximum value of the susceptibility in Eq. (3). The behavior of  $\chi$  at criticality is  $\chi = L^{\gamma/\nu} \bar{\chi}(u)$ , where  $u = (\theta - \theta_{c,k})L^{1/\nu}$  and  $\bar{\chi}$  is the corresponding scaling function. At the point where  $\chi$  is maximal,  $u = \text{const}$  and  $\chi_{\max} \propto L^{\gamma/\nu}$ . The data for  $\chi_{\max}$  with  $k = 2$  (squares) and  $k = 4$  (circles) are shown in Fig. 9(b). The obtained values of the slopes ( $\gamma/\nu$ ) are consistent with the exact value of the critical exponent of the ordinary percolation,  $\gamma = 43/18$ .

And, finally, the exponent  $\beta$  can be determined from the scaling behavior at criticality of the order parameter in Eq. (2):  $P = L^{-\beta/\nu} \bar{P}(u')$ , where  $u' = |\theta - \theta_{c,k}|L^{1/\nu}$  and  $\bar{P}$  is the scaling function. At the point where  $dP/d\theta$  is maximal,  $u' = \text{const}$  and  $(\frac{dP}{d\theta})_{\max} = L^{(-\beta/\nu+1/\nu)} \bar{P}(u') \propto L^{(1-\beta)/\nu}$ .

The scaling of  $(dP/d\theta)_{\max}$  is shown in Fig. 9(c) for  $k = 2$  and 4 as indicated. The values of  $\beta$  obtained from the slopes of

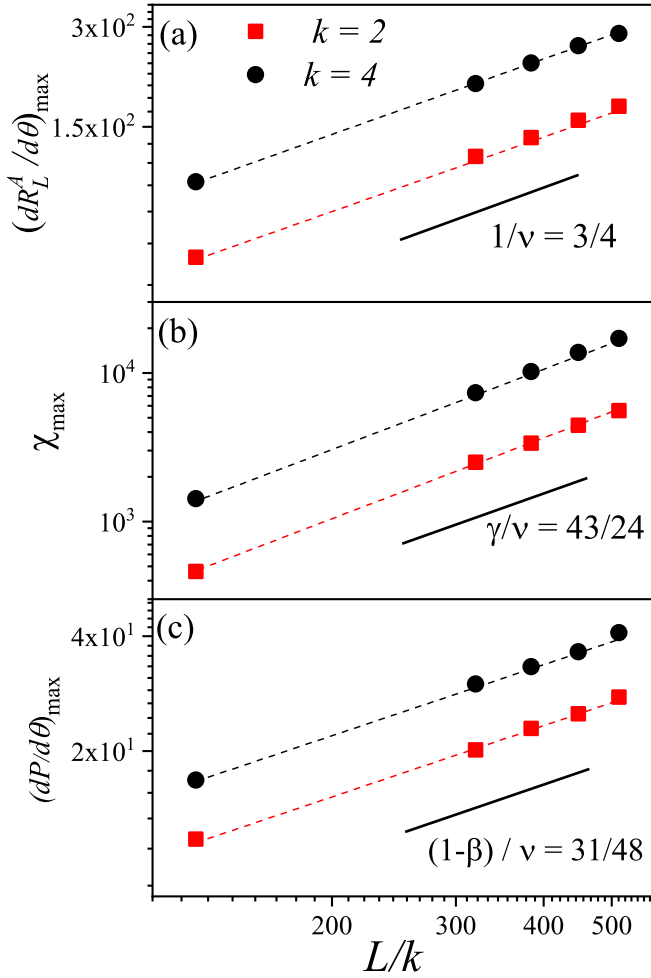


FIG. 9. (a) Log-log plot of  $(dR_{L,k}^A/d\theta)_{\max}$  as a function of  $L/k$  for two different cases:  $k = 2$  (circles) and  $k = 4$  (squares). According to Eq. (6), the slope of each line corresponds to  $1/\nu = 3/4$ . (b) Log-log plot of  $\chi_{\max}$  as a function of  $L/k$  for the cases in part (a). The slope of each line corresponds to  $\gamma/\nu = 43/24$ . (c) Log-log plot of  $(dP/d\theta)_{\max}$  as a function of  $L/k$  for the same cases reported in parts (a) and (b). The slope of each line corresponds to  $(1 - \beta)/\nu = 31/48$ .

the curves coincide (within the statistical error) with the exact value of  $\beta$  for ordinary percolation,  $\beta = 5/36$ .

The analysis carried out in Fig. 9 was repeated for  $k$  varying between 2 and 17. For each  $k$ , the values of  $\nu$ ,  $\gamma$ , and  $\beta$  were determined from the corresponding linear regressions. Combining these estimates, the average values of the critical exponents were calculated:  $\nu = 1.341(11)$ ,  $\gamma = 2.411(33)$ , and  $\beta = 0.138(9)$ . The results obtained for  $\nu$ ,  $\gamma$ , and  $\beta$  clearly indicate that the inverse percolation model in the bilayer square lattice belongs to the same universality class as random percolation regardless of the size of  $k$  considered.

When inverse percolation is considered both on the monolayer [17,25,26] and on the bilayer (this work), the analysis of the critical exponents shows that the problem belongs to the random percolation universality class. The latter is not the case for the drilling percolation model [35–37], which presents a different universality class than the ordinary random percolation model.

#### IV. CONCLUSIONS

The problem of inverse percolation by removing semirigid rods of length  $k$  ( $k$ -mers) from  $L \times L$  square lattices has been studied by numerical simulations and finite-size analysis. The process starts with the deposition of  $2L^2$  monomers forming two layers. In this initial configuration, all lattice sites are occupied and, consequently, the opposite sides of the lattice are connected by nearest-neighbor occupied sites. Then the  $L \times L \times 2$  system is diluted by removing groups of  $k$  consecutive nearest-neighbor monomers (aligned along one of two lattice axes) following a generalized random sequential adsorption (RSA) mechanism. The removed rods include semirigid  $k$ -mers whose components may be in both layers.

First, the dependence of the jamming coverage  $\theta_{j,k}$  on the size  $k$  was studied. It was demonstrated that the removal process of semirigid  $k$ -mers from the bilayer lattice  $L$  is equivalent to a RSA process of semirigid  $k$ -mers on the complementary bilayer lattice  $L^*$ . Each empty (occupied) site of  $L$  transforms into an occupied (empty) one of  $L^*$  and the first (second) layer in  $L$  corresponds to the second (first) layer in  $L^*$ . On the basis of these arguments, it is straightforward to conclude that  $\theta_{j,k} \equiv 1 - \theta_{j,k}^*$ , where  $\theta_{j,k}^*$  represents the limit concentration threshold for the standard (RSA) deposition of semirigid  $k$ -mers on a bilayer square lattice. Then, using the expression obtained for  $\theta_{j,k}^*$  in Ref. [27], it was found that  $\theta_{j,k} = 0.2701 + 0.062/k - 3.54/k^2$ . According to this equation, the jamming coverage  $\theta_{j,k}$  rapidly increases for small values of  $k$  and asymptotically converges towards a definite value for infinitely large  $k$ -sizes  $\theta_{j,k \rightarrow \infty} \approx 0.2701$ .

Once the limiting parameters  $\theta_{j,k}$  were determined, the percolation properties of the system were studied. It was found that the percolation threshold  $\theta_{c,k}$  decreases monotonically with increasing  $k$  up to  $k = 17$ . For  $k \geq 18$ , all jammed configurations are percolating states and, consequently, the percolation phase transition disappears. This implies that, for larger values of  $k$ , the jamming critical concentration occurs before the percolation phase transition and the system cannot be disconnected even when the highest allowed concentration of removed sites is reached.

The crossing between the percolation and jamming curves around  $k = 17$  and the absence of percolation phase transition for  $k \geq 18$  contrast sharply with the behavior observed for the standard RSA of semirigid  $k$ -mers on square lattices forming two layers. In the deposition case, percolating and nonpercolating phases extend to infinity in the space of the parameter  $k$  and the model presents percolation transition for the whole range of  $k$ . This finding indicates that, contrary to what was observed in the jamming case (where standard and inverse models are trivially symmetric,  $\theta_{j,k} + \theta_{j,k}^* = 1$ ), the complementarity property is not valid for percolation:  $\theta_{c,k} + \theta_{c,k}^* \neq 1$  ( $k > 1$ ). In fact, the cluster analysis for standard percolation is carried out in a phase of deposited rods. On the other hand, for inverse percolation, the cluster analysis is carried out in a phase of monomers, which remain in the lattice after the removal of a given number of  $k$ -mers. For  $k = 1$ , and as a consequence of the particle-hole symmetry characterizing the usual single-particle statistics, standard and inverse percolation are simply related:  $\theta_{c,k=1} + \theta_{c,k=1}^* = 1$ . However,

if some sort of correlation exists, like particles that occupy several contiguous lattice sites, the particle-hole symmetry is missing and standard and inverse percolation are completely independent problems. In other words, the inverse percolation problem cannot be derived straightforwardly from the standard percolation problem and it deserves a detailed treatment as presented here. This behavior had already been observed for the monolayer problem on the square lattice [17,26].

The results obtained here were also compared with the ones corresponding to the inverse percolation problem by removing rigid linear  $k$ -mers from a square monolayer [17]. The curve determining the lower boundary of the percolating region for the bilayer problem remains below the limit curve obtained for the monolayer problem. In terms of vulnerability and network attacks, this behavior indicates that the square monolayer is more vulnerable than the square bilayer to removal of linear sets of consecutive nodes. Moreover, for large  $k$ -mers ( $k > 17$ ), the bilayer lattice remains connected even when the highest allowed concentration of removed sites is reached. The present study reinforces the concept that the vulnerability of a network depends on its structure and the shape and size of the attacked region.

The present study complements previous research findings obtained for the monolayer problem [17] and could have potential application in the field of conductive films. The results in this paper, and those in Ref. [17], demonstrate that the possibility of forming a bilayer favors the connectivity of the system against the failure of single network components. Thus our theoretical predictions can guide future experiments investigating the effects of multilayer deposition or removal of conductive elements on the conductive properties of the resulting system.

As it was mentioned in the Introduction, the bilayer may resemble the multilayer networks but there are several differences in the behavior of both systems. Studies on attacks in single complex networks have shown that percolation transitions are second-order transitions [20,21]. The robustness of single networks strongly depends on their degree distribution. For instance, Erdős-Rényi networks with homogeneous connectivity are highly susceptible to random failures or attacks, whereas scale-free networks with heterogeneous connectivity demonstrate exceptional resilience to them but are more sensitive to targeted attacks [44,45]. In contrast, percolation in multiplex networks leads to a first-order transition [30,34,46] and is extremely vulnerable to random removal of nodes, even when broader degree distributions are considered [30]. Real multilayer networks have also been studied and it has been found that they can be resilient to targeted attacks

on high degree nodes due to their hidden interlayer geometric correlations. In contrast, multiplex networks without such correlations are extremely vulnerable to these attacks [29]. It is also noteworthy that a single layer is found to be more resilient to random failures than the multilayer [30,34,46], whereas here the bilayer is more robust than the monolayer.

The complete set of critical exponents  $\nu$ ,  $\beta$ , and  $\gamma$  was determined. The results obtained confirm that the percolation phase transition involved in the system, which occurs for  $k$  varying between 1 and 17, belongs to the same universality class as the standard two-dimensional percolation problem. Even though the bilayer geometry of the lattice drastically affects the behavior of the percolation threshold as a function of the  $k$ -mer size, it does not alter the nature of the percolation transition occurring in the system as in the drilling percolation problem [35–37].

Future efforts will be devoted to (i) extending the present analysis to  $n$ -layer systems with  $n > 2$  and removed rods of sizes  $k$  of the order of  $L$  (under these conditions, the results obtained could be analyzed in terms of drilling percolation), (ii) exploring the asymmetry between standard and inverse percolation in other 2D lattices (honeycomb, triangular), and (iii) investigating the effect of the shape of the removed object (structure of the attack) on the connectivity properties of the diluted (damaged) lattice.

#### ACKNOWLEDGMENTS

This work was supported in part by CONICET (Argentina) under Project No. PIP 112-201101-00615, Universidad Nacional de San Luis (Argentina) under Project No. 03-1920, and Ministry of Higher Education, Science and Technology, MESCYT-Dominican Republic, under Project No. FONDOCYT-2020-2021-1A2-112. The numerical work was done using the BACO parallel cluster located at Instituto de Física Aplicada, Universidad Nacional de San Luis–CONICET, San Luis, Argentina. L.S.R. acknowledges the Juan de La Cierva program (reference FJC2021-046559-I) funded by MCIN/AEI/10.13039/501100011033 and European Union Next Generation EU/PRTR, and also financial support has been received from the Agencia Estatal de Investigación (AEI, MCI, Spain) MCIN/AEI/10.13039/501100011033 and Fondo Europeo de Desarrollo Regional (FEDER, UE) under Project APASOS (PID2021-122256NB-C21/C22) and the María de Maeztu Program for units of Excellence in R&D, Grant No. CEX2021-001164-M.

- 
- [1] G. Grimmett, *Percolation* (Springer-Verlag, Berlin, 1999).
  - [2] B. Bollobás and O. Riordan, *Percolation* (Cambridge University Press, New York, 2006).
  - [3] D. Stauffer and A. Aharony, *Introduction to Percolation Theory* (Taylor & Francis, London, 2003).
  - [4] J. W. Evans, *Rev. Mod. Phys.* **65**, 1281 (1993).
  - [5] P. L. Krapivsky, S. Redner, and E. Ben-Naim, *A Kinetic View of Statistical Physics* (Cambridge University Press, Cambridge, UK, 2010).
  - [6] M. Nakamura, *J. Phys. A: Math. Gen.* **19**, 2345 (1986).
  - [7] M. Nakamura, *Phys. Rev. A* **36**, 2384 (1987).
  - [8] A. J. Ramirez-Pastor, P. M. Centres, E. E. Vogel, and J. F. Valdés, *Phys. Rev. E* **99**, 042131 (2019).
  - [9] A. C. Buchini Labayen, P. M. Centres, P. M. Pasinetti, and A. J. Ramirez-Pastor, *Phys. Rev. E* **100**, 022136 (2019).
  - [10] Y. Y. Tarasevich, N. I. Lebovka, and V. V. Laptev, *Phys. Rev. E* **86**, 061116 (2012).
  - [11] G. Kondrat, Z. Koza, and P. Brzeski, *Phys. Rev. E* **96**, 022154 (2017).

- [12] M. G. Slutskiĭ, L. Y. Barash, and Y. Y. Tarasevich, *Phys. Rev. E* **98**, 062130 (2018).
- [13] L. S. Ramirez, P. M. Pasinetti, W. Lebrecht, and A. J. Ramirez-Pastor, *Phys. Rev. E* **104**, 014101 (2021).
- [14] G. A. Iglesias Panuska, P. M. Centres, and A. J. Ramirez-Pastor, *Phys. Rev. E* **102**, 032123 (2020).
- [15] P. M. Pasinetti, P. M. Centres, and A. J. Ramirez-Pastor, *J. Stat. Mech.* (2019) 103204.
- [16] G. D. García, F. O. Sanchez-Varretti, P. M. Centres, and A. J. Ramirez-Pastor, *Eur. Phys. J. B* **86**, 403 (2013).
- [17] L. S. Ramirez, P. M. Centres, and A. J. Ramirez-Pastor, *J. Stat. Mech.* (2015) P09003.
- [18] S. N. Dorogovtsev and J. F. F. Mendes, *Evolution of Networks: From Biological Nets to the Internet and WWW* (Oxford University Press, Oxford, UK, 2003).
- [19] M. E. J. Newman, A.-L. Barabási, and D. J. Watts, *The Structure and Dynamics of Networks* (Princeton University Press, Princeton, NJ, 2006).
- [20] M. E. J. Newman, *Networks: An Introduction* (Oxford University Press, Oxford, UK, 2010).
- [21] R. Cohen and S. Havlin, *Complex Networks, Structure, Robustness and Function* (Cambridge University Press, Cambridge, UK, 2010).
- [22] Y. Kornbluth, S. Lowinger, G. A. Cwilich, and S. V. Buldyrev, *Phys. Rev. E* **89**, 032808 (2014).
- [23] S. Lowinger, G. A. Cwilich, and S. V. Buldyrev, *Phys. Rev. E* **94**, 052306 (2016).
- [24] H. Hinrichsen, *Adv. Phys.* **49**, 815 (2000).
- [25] L. S. Ramirez, P. M. Centres, and A. J. Ramirez-Pastor, *J. Stat. Mech.* (2017) 113204.
- [26] L. S. Ramirez, P. M. Centres, and A. J. Ramirez-Pastor, *Phys. Rev. E* **100**, 032105 (2019).
- [27] N. De La Cruz Félix, P. M. Centres, and A. J. Ramirez-Pastor, *Phys. Rev. E* **102**, 012153 (2020).
- [28] M. Kivelä *et al.*, *J. Complex Networks* **2**, 203 (2014).
- [29] K.-K. Kleineberg, L. Buzna, F. Papadopoulos, and M. Boguñá, and M. A. Serrano, *Phys. Rev. Lett.* **118**, 218301 (2017).
- [30] S. V. Buldyrev, R. Parshani, G. Paul, H. E. Stanley, and S. Havlin, *Nature (London)* **464**, 1025 (2010).
- [31] J. Gao, S. V. Buldyrev, H. E. Stanley, and S. Havlin, *Nat. Phys.* **8**, 40 (2012).
- [32] B. Min, S. D. Yi, K.-M. Lee, and K.-I. Goh, *Phys. Rev. E* **89**, 042811 (2014).
- [33] S. Osat, A. Faqeeh, and F. Radicchi, *Nat. Commun.* **8**, 1540 (2017).
- [34] J. Shao, S. V. Buldyrev, S. Havlin, and H. E. Stanley, *Phys. Rev. E* **83**, 036116 (2011).
- [35] K. J. Schrenk, M. R. Hilário, V. Sidoravicius, N. A. M. Araújo, H. J. Herrmann, M. Thielmann, and A. Teixeira, *Phys. Rev. Lett.* **116**, 055701 (2016).
- [36] P. Grassberger, *Phys. Rev. E* **95**, 010103(R) (2017).
- [37] P. Grassberger, M. R. Hilário, and V. Sidoravicius, *J. Stat. Phys.* **168**, 731 (2017).
- [38] J. Hoshen and R. Kopelman, *Phys. Rev. B* **14**, 3438 (1976).
- [39] F. Yonezawa, S. Sakamoto, and M. Hori, *Phys. Rev. B* **40**, 636 (1989).
- [40] K. Binder, *Rep. Prog. Phys.* **60**, 487 (1997).
- [41] S. Biswas, A. Kundu, and A. K. Chandra, *Phys. Rev. E* **83**, 021109 (2011).
- [42] A. K. Chandra, *Phys. Rev. E* **85**, 021149 (2012).
- [43] N. Vandewalle, S. Galam, and M. Kramer, *Eur. Phys. J. B* **14**, 407 (2000).
- [44] R. Cohen, K. Erez, D. ben-Avraham, and S. Havlin, *Phys. Rev. Lett.* **85**, 4626 (2000).
- [45] D. S. Callaway, M. E. J. Newman, S. H. Strogatz, and D. J. Watts, *Phys. Rev. Lett.* **85**, 5468 (2000).
- [46] R. Parshani, S. V. Buldyrev, and S. Havlin, *Phys. Rev. Lett.* **105**, 048701 (2010).